

Patterned Block-Copolymer-Silica Mesostructures as Host Media for the Laser Dye Rhodamine 6G

Gernot Wirnsberger,[†] Peidong Yang,^{†,||} Howard C. Huang,^{†,‡} Brian Scott,[†] Tao Deng,[§] George M. Whitesides,[§] Bradley F. Chmelka,[‡] and Galen D. Stucky^{*,†}

Department of Chemistry, University of California, Santa Barbara, California 93106, Department of Chemical Engineering, University of California, Santa Barbara, California 93106, and Department of Chemistry and Chemical Biology, Harvard University, Cambridge, Massachusetts 02138

Received: March 14, 2001

Rhodamine 6G-doped mesostructured silica is prepared by an acidic sol–gel route using poly-*b*-poly(propylene oxide)-*b*-poly(ethylene oxide) (EO_{*x*}–PO_{*y*}–EO_{*x*}) block copolymer surfactants. Using low-refractive-index ($n \sim 1.2$) mesoporous SiO₂ as a support, the synthesis is combined with soft lithography to produce high-quality waveguides. This enables efficient waveguiding in the line-patterned rhodamine 6G-doped mesostructured domains, which have a higher refractive index than both the mesoporous support and cladding. For the structure-directing block copolymer surfactants used, (EO)₂₀(PO)₇₀(EO)₂₀ (P123) and (EO)₁₀₆(PO)₇₀–(EO)₁₀₆ (F127), X-ray diffraction patterns and transmission electron microscopy reveal hexagonal mesophases, whose longitudinal cylinder axes are aligned predominantly parallel to the substrate plane. For samples made by micromolding-in-capillaries (MIMIC), the longitudinal axes are also aligned along the longitudinal waveguide axes. Samples made by micromolding also possess a high mesostructural order, though in the absence of an aligning flow field, their long-range order (ca. several hundred nanometers) is lower than for samples processed using the MIMIC technique. When optically pumped, the rhodamine 6G-doped waveguides exhibit amplified spontaneous emission with thresholds as low as $\sim 6 \text{ kW cm}^{-2}$, substantially lower than rhodamine 6G-doped sol–gel glasses. This is attributed to the ability of the polymeric surfactant to co-assemble with the dye molecules, thereby leading to high dye dispersions and reduced dye dimerization. Additionally, rhodamine 6G shows good photostability in the mesostructured waveguides, similar to that of rhodamine 6G in organically modified silicates.

Introduction

In recent years, mesostructured/mesoporous materials^{1–3} have attracted a great deal of interest as potential catalysts and separation media,^{4–6} because of their large pore dimensions and volumes and high internal surface areas. Other interesting application possibilities exist for mesoscopically ordered composites as optical materials, particularly as host media for molecules and complexes exhibiting optical functionalities.^{7,8} Such materials, with symmetric and adjustable mesoscopic structures and compositions, offer new opportunities for controlling the local environments of occluded dye molecules. Until now, dye inclusion has been mainly restricted to either incorporation in pure oxides (e.g., refs 9–12) or other polymeric hosts such as NAFION and organic polymers (e.g., refs 13–16). An exception is the occlusion of dyes in organically modified silicates (ORMOSILs), which have been shown to allow structural tuning of the local dye environment to a certain degree.^{17,18} In this context, very recently, sol–gel glasses have also been doped with surfactants and their use has been shown to influence substantially the spectroscopic properties of simultaneously occluded dye molecules.¹⁹ The degree of control over dye molecule environments and other advantages such as

enhanced photostability of occluded dye species is expected to be significantly enhanced in dye-doped mesostructured composites. Furthermore, it is likely that new synergistic effects might result from surfactant/dye co-assembly into mesoscopically ordered structures. The use of nonionic, cationic, or anionic surfactants²⁰ and the possibility of preparing structures under basic, neutral, or acidic conditions^{2,3,21–24} offers versatile synthesis and processing conditions that can be used to tailor materials to desired properties. Silica mesostructured materials synthesized under acidic conditions^{22,25} below the pH \sim 2 isoelectric point of silica have proved to be particularly promising in that they can be rapidly processed into different morphologies such as fibers,^{7,8,26,27} thin films,^{28–33} monoliths,^{34,35} and hierarchically ordered structures.³⁶ Synthesis conditions can moreover be adapted to allow such materials to be prepared over a wide range of inorganic framework compositions and mesoscopic structures to tailor the properties of these complex heterogeneous multicomponent compounds.³⁷

Whereas the first incorporation of dye molecules into mesostructured materials was aimed at in situ monitoring of mesostructure formation during processing,^{28,38} recent efforts have been directed toward the goal of obtaining dye-doped structures for optical applications.^{8,39,40} Quite different approaches have been used, ranging from the incorporation of phthalocyanins and specifically designed surfactants,⁴¹ or insertion of polymers into MCM-41-type materials after surfactant extraction,⁴² to the generation of photoluminescent silicon clusters on the walls of as-synthesized SBA-3 films.⁴³ We have

* Corresponding author. E-mail: stucky@chem.ucsb.edu.

[†] Department of Chemistry, University of California.

[‡] Department of Chemical Engineering, University of California.

[§] Department of Chemistry and Chemical Biology, Harvard University.

^{||} Present address: Department of Chemistry, University of California, Berkeley, CA 94720.

recently reported the development of patterned microlaser arrays formed from rhodamine 6G (R6G)-doped mesostructured silica using the amphiphilic triblock copolymer poly(ethylene oxide)-*b*-(polypropylene oxide)-*b*-poly(ethylene oxide) (EO)₂₀(PO)₇₀(EO)₂₀ (abbreviated P123).⁴⁴ R6G-doped mesostructured silica composites were formed into long nonintersecting line patterns by using soft lithography (for reviews on this topic see refs 45–47). In this article, we focus on a detailed characterization of these waveguides, addressing mesostructure alignment, waveguiding properties, photostability, the effect of dye concentration, and the use of different surfactants, namely P123 and (EO)₁₀₆(PO)₇₀(EO)₁₀₆ (abbreviated F127).

Experimental Section

Sample Preparation. Patterned dye-containing mesostructured waveguides were prepared on mesoporous silica thin film supports cast on a silicon surface, as follows. Solutions of the same composition previously used for mesostructured (-porous) film preparation by dip-coating³³ were spin-coated on silicon wafers (2000 rpm) to produce films with thicknesses of about 1 μm. These films were calcined by heating them to 673 K within 4 h and holding them at this temperature for 4 h. After cooling, the waveguide structures were patterned on top of these films by soft lithographic methods using polydimethylsiloxane (PDMS) molds to organize macroscopically a polymerizing silica sol–gel mixture in the presence of mesostructure-directing P123 triblock copolymer species. For the patterning of dye-doped waveguide arrays, the block copolymer-silica mesophases had the following compositions: P123:tetraethoxysilane (TEOS):EtOH:H₂O:HCl:R6G = 0.0172:1.00:22.15:5.00:0.02:0.001–0.006 (in molar ratios). Solutions were prepared by combining P123, EtOH, H₂O, HCl, and TEOS and refluxing the resulting clear solution for 1 h. After the solution had been cooled to room temperature, R6G was added and the solution was stirred for an additional hour. For the waveguides prepared with F127 the same weight of surfactant was used as in the P123 preparations. The molar composition was F127:TEOS:EtOH:F127:H₂O:HCl:R6G = 0.0079:1.00:22.15:5.00:0.02:0.001–0.006. For materials synthesized using either P123 or F127, the concentration of the R6G dye species was varied, ranging from about 0.25 wt % to 1.5 wt % in the final solid. The final R6G concentrations in the solids are reported with respect to the amount of P123 and SiO₂ and assuming that TEOS fully hydrolyzed and condensed into SiO₂.

Patterning was performed by using either micromolding or micromolding-in-capillaries (MIMIC) techniques to produce surface replicas of the relief patterns of the PDMS mold.^{45–47} For micromolding, a drop of the solution described above was placed on the mesoporous silica film support, covered by a stripe-patterned PDMS mold, and a slight pressure applied to dewet the surfaces between the individual stripes. In the case of MIMIC, the PDMS mold was first placed on the mesoporous silica film support, a drop of solution was placed at both ends of the mold, and the line arrays were allowed to fill by capillary flow.⁴⁵ No cleanroom facilities were used during the waveguide preparations.

Characterization Measurements. Prior to characterization, the waveguide patterns were cleaved to remove thick corrugated regions that formed near the edges of the PDMS patterns. X-ray diffraction (XRD) patterns were obtained on a Scintag PAD X diffractometer employing Cu Kα radiation. Scanning electron micrographs (SEM) were recorded on a JEOL 6300-F after sputtering the samples with gold. Transmission electron microscopy (TEM) was performed a JEOL 2000 FX after

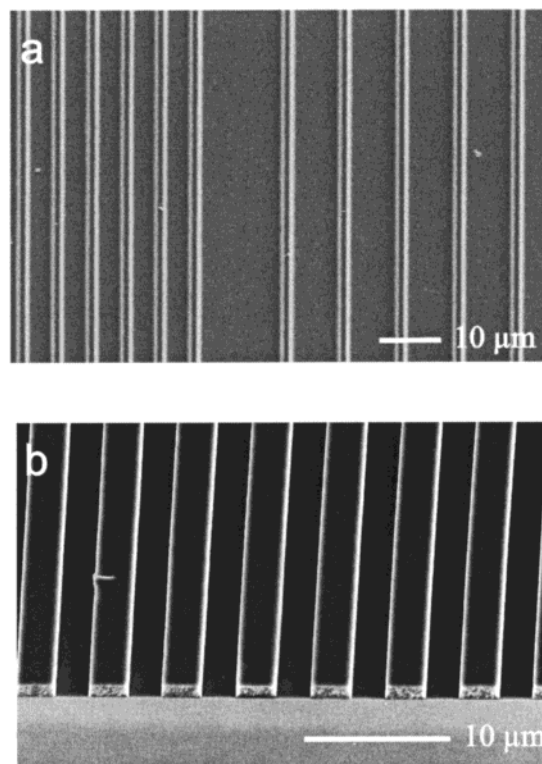


Figure 1. SEM image showing (a) mesostructured waveguide patterns having different spacings and (b) the waveguide ends after cleaving the substrate. Note the relatively high smoothness of the cleaved edges.

calcination of the samples at 673 K for 4 h. Film thicknesses were measured with a DEKTAK profiler. Photoluminescence spectra were recorded in a 90° setup. These measurements were performed using light from the second harmonic of a Q-switched Nd:YAG laser (532 nm, about 10 ns pulse width, 10 Hz repetition rate), which was passed through calibrated neutral density filters and an adjustable slit and focused by a rectangular lens onto the sample (typically to an area of 2 mm × 0.5 mm). Light emerging from the end of the waveguides was collected by a set of two lenses and focused on the entrance slit of a 0.25 m monochromator (150 groves/mm). For signal detection, a liquid nitrogen cooled CCD detector was used. As a rule, the waveguide patterns were used for measurements in the time interval of some hours to 3 days after their preparation.

Results and Discussion

Mesostructural Ordering and Alignment. Both the micromolding and MIMIC methods for producing patterned mesostructured waveguides led to arrays of several-millimeter-long stripe features with smooth surfaces and only occasional defects, as shown in the SEM images of Figure 1. By using PDMS molds with different line spacings, the distances between the individual waveguides can be adjusted (Figure 1a). Furthermore, it is also feasible to produce waveguides with different cross-sections such as, for example, rectangular or trapezoidal shapes. The high surface qualities of the line patterns demonstrated in Figure 1b are essential for achieving low-loss waveguiding. Note also that cleavage of the waveguides perpendicular to the long axes of the waveguides after synthesis generally results in relatively well-defined front faces (Figure 1b).

Using P123 as the structure-directing surfactant species and MIMIC to form the line patterns, highly ordered mesostructured waveguides can be produced. As shown in Figure 2a, the corresponding XRD patterns exhibit as many as five (*h*00)

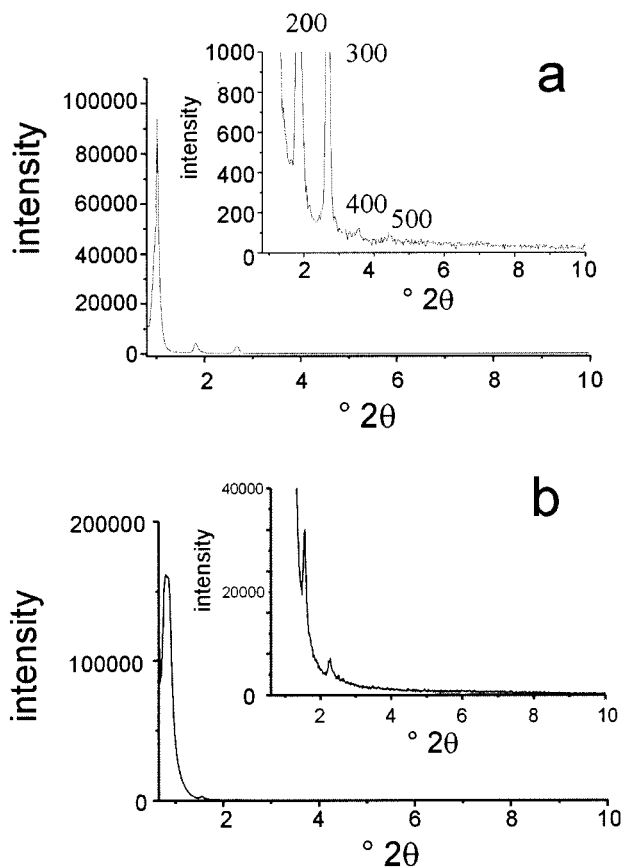


Figure 2. XRD patterns of waveguide arrays synthesized with (a) P123 and (b) F127 block copolymer surfactant species.

reflections ($d_{100} = 92 \text{ \AA}$). This XRD pattern is similar to that observed for SBA-15 films³³ and is due to a high degree of ordering and strong preferred orientation of the channels parallel to the substrate plane. Under the conditions used here, P123 strongly favors a hexagonal phase with $p6mm$ symmetry,^{25,33} as confirmed for these materials using TEM (Figure 3a, top). For samples produced using the MIMIC method, TEM (Figure 3a, bottom) also shows extended arrays of well-ordered regions of parallel channels, which extend over several micrometers and which are hence longer than the $\sim 1.5 \mu\text{m}$ cross section of the waveguides. The uniaxial capillary flow results in a preferred alignment of the channels not only parallel to the substrate plane but also parallel to the long axis of the waveguides. This finding is in agreement with previous studies of the orientational ordering of aggregates in line patterns during the synthesis of SBA-3 prepared with the low-molecular-weight amphiphilic surfactant cetyltrimethylammoniumbromide (CTAB) and MIMIC in electric fields.⁴⁸ XRD patterns were similar when micro-molding and P123 were used for the preparation of the waveguides. However, TEM inspection shows that these samples are not as well ordered on a length scale of several hundred nanometers as samples synthesized using MIMIC.

In contrast to P123, which tends to form hexagonal structures with $p6mm$ symmetry, co-assembly of F127 with silica under acidic conditions can lead to cubic or a hexagonal structures.^{33,34} As shown in Figure 2b, XRD patterns for the waveguides made with F127 show one strong reflection at a d spacing of 114 \AA and two weaker higher order reflections at 56 and 38 \AA . TEM images in Figure 3b show regions that indicate a 2-d hexagonal structure ($p6mm$), which is consistent with the XRD pattern in Figure 2b. Similar to the waveguides prepared using P123, MIMIC results in F127/silica waveguides that have excellent

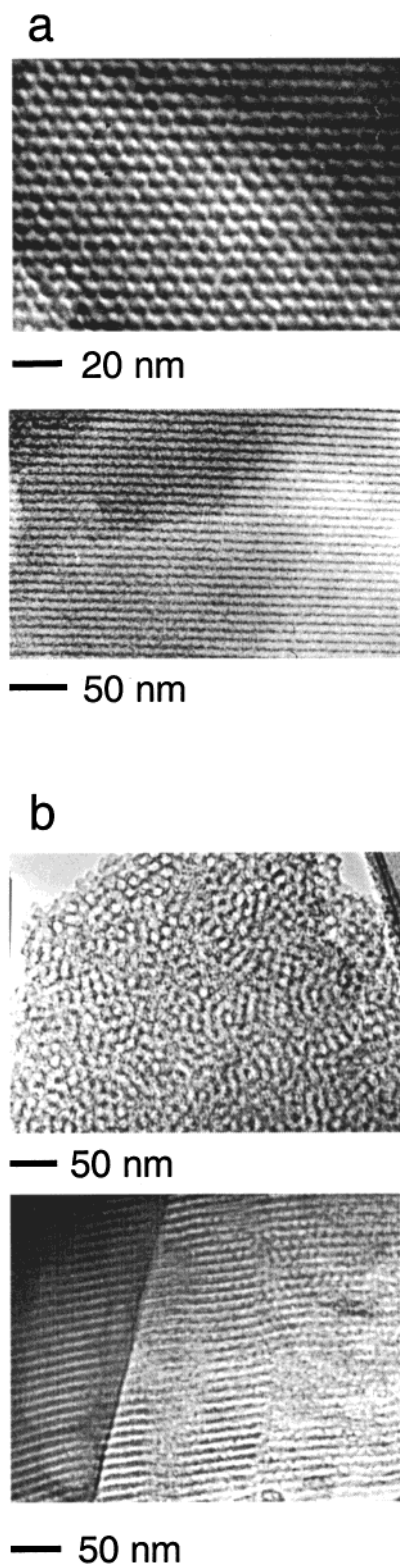


Figure 3. (a) TEM images of mesostructured waveguides (after calcination). The samples were prepared with (a) P123 and (b) F127 triblock-copolymer species.

long-range order, again indicative of a channel alignment parallel to the waveguide axes. However, on a longer length scale of several hundred nm, ordering appears to be somewhat less than when micromolding is used.

Under capillary flow conditions, the cylindrical aggregates of the hexagonal mesostructure orient along the flow direction, as similarly found for dip-coated films.³³ This is not the case when samples are prepared by the micromolding technique,

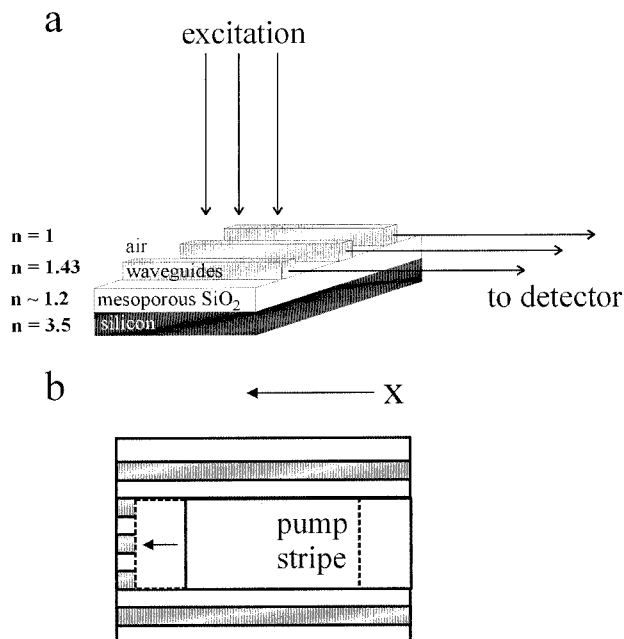


Figure 4. (a) Schematic representation of the mesoporous support-mesostructured waveguide architecture. The illustration also depicts the measuring geometry used. (b) Illustration of the loss measurements. The pump stripe is moved the distance x from the edge apart, and the output is monitored with the spectrometer.

where the cylindrical aggregates align mainly parallel to the substrate plane, but are less well orientationally ordered in the absence of the additional capillary shear flow field.

Amplified Spontaneous Emission. Due to the low refractive index of the mesostructured block-copolymer-silica waveguides ($n = 1.43$), waveguiding cannot be achieved on supports with higher indices of refraction, such as commonly used silicon ($n = 3.5$) or silica glass ($n = 1.51$). However, mesostructured block-copolymer-SiO₂ thin films can be conveniently deposited by spin coating to produce films with thicknesses of about 0.5 μm after calcination. XRD patterns of as-synthesized films show several d_{h00} peaks indicative of a preferred alignment of the hexagonal structure in the film plane,³³ which is preserved following calcination, though ordering is diminished. The thin supporting films are mesoporous and possess low refractive indices $n = 1.15$ to 1.3, depending on the porosity. Waveguiding results within the composite line patterns from internal reflection of light at the lower refractive index mesoporous SiO₂ and the air interfaces. Waveguide modeling shows that several modes can be supported in this step-index waveguide structure. Figure 4a depicts this multilayer structure schematically, together with the measurement geometry.

When the R6G-doped waveguides are pumped with the second harmonic of a Nd:YAG laser (532 nm) in a 90° geometry (Figure 4a), at low intensities a broad photoluminescence spectra is observed with a full width at half-maximum (fwhm) of around 50 nm. As the pump intensity increases, however, the spectra begin to narrow and finally a gain-narrowed band with a fwhm of 7–8 nm is obtained (Figure 5a). A typical dependence of the output intensity with increasing laser power is depicted in Figure 5b for a sample synthesized with P123 and containing a concentration of R6G in the solid of about 0.58 wt %. From these data, a low threshold⁴⁹ of about 25 kW cm^{-2} is deduced. As no cavity is present, the observed effects are indicative of amplified spontaneous emission (ASE), an effect in which spontaneously emitted light is amplified as it propagates along the waveguide.^{50,51} To establish unambiguously

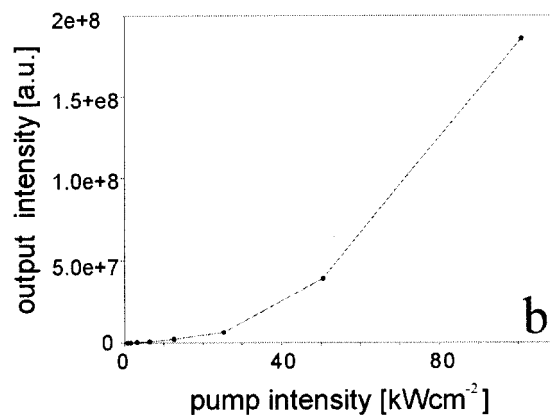
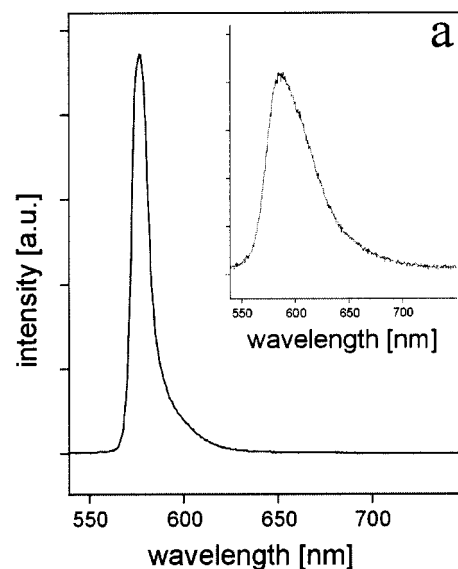


Figure 5. (a) Emission spectra of R6G-doped waveguides below and above the threshold. The inset shows the broad luminescence spectrum at low pumping energies ($\sim 1 \text{ kW cm}^{-2}$). (b) Output vs pump intensity for mesostructured waveguides (surfactant = P123, R6G-concentration = 0.58 wt %):

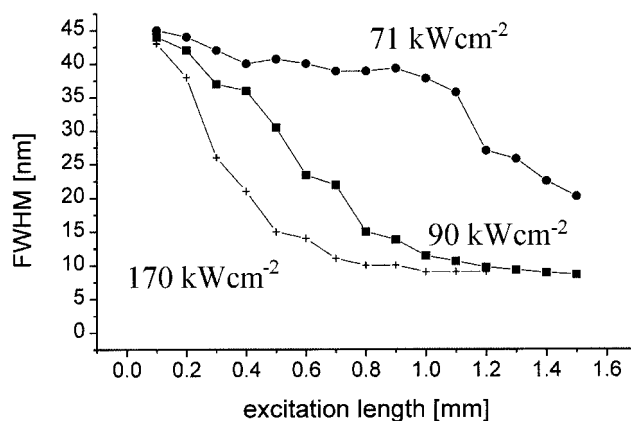


Figure 6. Full width at half-maximum of the R6G luminescence spectra as a function of the excitation strip length and excitation energy (surfactant = P123, R6G-concentration = 0.58 wt %).

that the observed gain-narrowing behavior is due to ASE, a type of mirrorless lasing,⁵⁰ we performed a variable stripe experiment, in which the length of the excitation stripes were varied.^{52,53} The results in Figure 6 clearly show that the gain-narrowing is dependent on the excitation stripe length and confirm its origin as resulting from ASE. For a certain energy, e.g., 90 kW cm^{-2} ,

the spectra narrow with increasing power until no further gain-narrowing occurs, and the fwhm remains constant despite a further increase in the excitation length stripe. As several low-order modes can in principle be supported, the ASE light does not show a large polarization dependence; the ratio of the light being polarized parallel to the substrate plane versus that being polarized normal to the substrate plane is approximately 6. Below threshold the value is ~ 1 .

The loss in the R6G-doped mesostructured silica waveguides at the ASE wavelength was determined by moving the excitation stripe from the end (Figure 4b) and monitoring the output emerging from the end of the waveguides.⁵⁴ In these experiments, the energy was well above the threshold. The intensity, I , of the ASE light emerging from the end of the waveguides when the excitation stripe is moved a distance, x , from the end (see Figure 4b) is given by $I = I_0 e^{-\alpha x}$ where I_0 is the output intensity when the excitation stripe is focused just on the end and α is the loss in cm^{-1} . Loss measurements were performed on 10 different waveguide patterns, which consistently yielded loss values between 16 and 25 cm^{-1} from the fits. These values, at the ASE wavelength, are smaller than values reported for pure semiconducting polymers (20, 44, and 90 cm^{-1}),^{53,54} but higher than those for polymer blends where energy transfer is employed (values between 1 cm^{-1} and 7 cm^{-1}).^{54,55} The losses in the block-copolymer-silica waveguides are attributed to several factors. First, at the ASE wavelength, R6G molecules still absorb energy (self-absorption), albeit with a lower absorption cross-section. Second, the supporting thin films sometimes exhibit bubble-like defects (in the nanometer to micrometer size range), which can act as scattering centers in the waveguides. Whereas the presence of defects can be reduced by improved processing, self-absorption is an intrinsic problem that is important from an application point of view.

Photostability. An important characteristic performance property of laser systems is their lifetime. To address this issue, we have monitored the output intensity vs time (pulses) for different pump intensities and pumping rates over a period of several thousand pulses. The photostability depends on both pump intensity and frequency. At the same frequency, a lower pump intensity results in enhanced lifetime. On the other hand, when the pump frequency is reduced from 10 to 2 Hz, even higher pump intensities can be maintained for a relatively long time. For example, at 1.7 MW cm^{-2} , a reduction to half of the original intensity output is observed after around 2500 pulses at a repetition rate of 2 Hz, even when the pump intensity is far above the energy required for fully gain-narrowed spectra (see Figure 7). Similar lifetimes are observed when the pumping power is reduced to 120 kW cm^{-2} but the repetition rate is increased to 10 Hz. It is interesting to compare the photostabilities of R6G incorporated in these hybrid silica/block copolymer systems with those of R6G in inorganic systems or sol-gel materials. Whereas the photostability of R6G has been reported to be very low under laser action in doped inorganic salts such as K_2SO_4 , it is enhanced in polymeric organic systems such as poly(methyl methacrylate) and sol-gel-derived oxide materials. An exact comparison is difficult, because different configurations (e.g., laser action by ASE or realization of a laser cavity) or macroscopic shapes of the samples (e.g., monoliths or thin films) have been used. However, the literature data generally reveal that the photostability of R6G is substantially better in sol-gel-derived Al_2O_3 and silica than in organic polymers.^{17,18} This was also evidenced in the only study of which we are aware that focused on the stability of four dyes in different hosts under nearly identical conditions.⁵⁶ Extensive

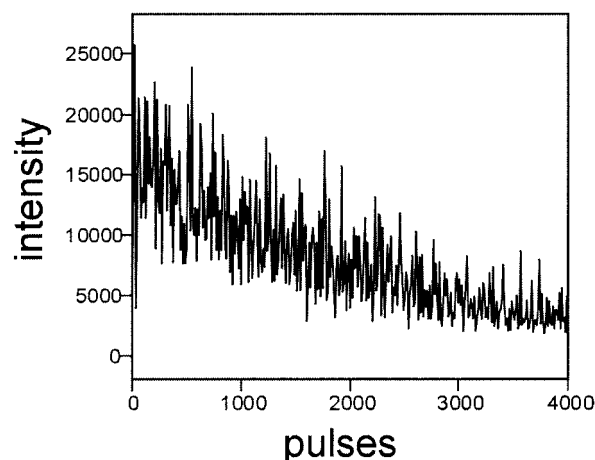


Figure 7. Output intensity vs number of pulses for pump intensities high above the threshold at a pumping energy of 1.7 MW cm^{-2} and a repetition rate of 2 Hz.

work during the past decade to improve photostability led to the development of ORMOSILs as dye host materials.^{17,18,57} Compared to these latter materials, dye-doped block-copolymer/silica waveguides possess similar photostabilities with a half-life of several thousand pulses. Further improvements may be possible by using dyes with better photostability than R6G or dyes that may be stabilized by interactions with the inorganic framework or the block copolymer surfactant species.

Effect of Dye Concentration and Surfactant. Besides improved photostability compared to purely organic or inorganic hosts, a further advantage of mesostructured materials is their better performance with regard to the ASE threshold. For comparison, we also prepared R6G-doped amorphous silica waveguides on mesoporous SiO_2 from the same starting composition by leaving out the surfactant and adjusting the dye concentration to the same level. Although these waveguides also have relatively low thresholds (approximately 200 kW cm^{-2}), they are more than an order of magnitude higher than those of the mesostructured compounds reported in this study. The thresholds of these surfactant-free silica waveguides are significantly higher than in the mesostructured waveguides and in cetyltrimethylammonium-derived mesostructured fibers.⁸ In agreement with these results, previous investigations on pure silica systems⁵⁶ and silica/titania thin films¹² report much higher thresholds with pumping energies in the mJ range. We attribute the low thresholds in our systems to the capability of the surfactant species to promote a high dye-dispersion and isolation, which reduces dimerization. This is supported by UV/vis spectra on thin R6G-doped mesostructured films, which show a much lower dimer absorption, in comparison with pure R6G-doped SiO_2 thin films.⁵⁸ Very recently, a high dye-dispersion has been proposed for phthalocyanin-doped small-pore mesostructured materials, as well.^{39,59,60} Although currently we cannot exclude that some small amount of the R6G is located within the silica walls, the experimental results indicate that the surfactant species appears to interact with the dye molecules, playing an important and beneficial role in preventing R6G aggregation. In a similar context, surfactants have long been used in solution to suppress dye dimerization.⁶¹

To assess the dispersion of R6G molecules in the block-copolymer/silica composites, we further increased the R6G concentration in the final solids. In this way, we could systematically lower the threshold to approximately 5 kW cm^{-2} (Figure 8). At the highest dye concentration (1.5 wt %), the gain-narrowing ceases at a higher fwhm of about 12–13 nm

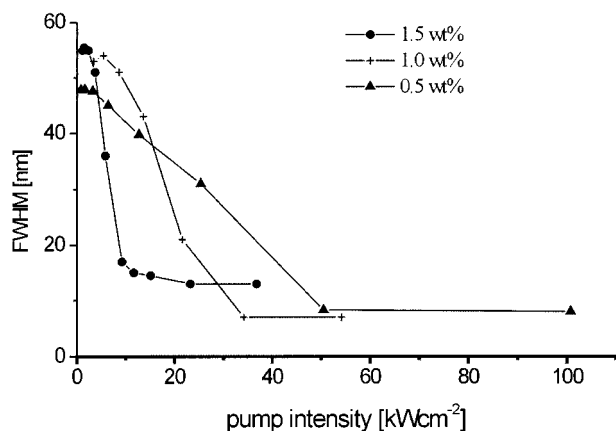


Figure 8. Dependence of full width at half-maximum (fwhm) of the luminescence spectra of R6G-doped mesostructured waveguides on the excitation energy for different concentrations of included R6G dye species.

(see Figure 8). The low thresholds observed are strong evidence that the surfactants promote higher dye dispersion, suppressing unfavorable dimerization and leading to mostly isolated R6G molecules. The threshold values compare well, even with the best polymers known to date: about $0.1\text{--}0.5\text{ kW cm}^{-2}$ (e.g., refs 54–56). Based on this first example of a low-threshold mesostructured material, it is likely that optimization of the composition, structure, and processing conditions of these systems will lead to further improvements in their optical properties and performance. One improvement to explore is the use of dyes having reduced self-absorption. Another possibility, which we are currently investigating, is employing energy transfer in mesostructured materials by doping with two lumophores simultaneously.⁵⁸

Another interesting point is to compare the systems prepared with F127 to those prepared with P123. For the former, thresholds on the order of $32\text{--}35\text{ kW cm}^{-2}$ are measured at a dye concentration of 0.58 wt %. This is around $7\text{--}10\text{ kW cm}^{-2}$ higher than for the corresponding P123-derived samples. The F127 surfactants, having longer hydrophilic poly(ethylene oxide) segments, lead to a slightly different local dye environment. As the R6G is hydrophilic, it is supposed to be located within the EO segments in the mesostructure. On the other hand, it has been shown that for monolithic F127/silica composites, the EO segments grow into the silica part. The more hydrophilic environment resulting may explain both the slightly higher thresholds as well as a shift of the maximum of the luminescence spectra from 586 nm in P123-based composites to 576 nm in F127-based materials.

Conclusions

High-quality mesostructured waveguides can be prepared rapidly by combining soft lithographic methods with acidic sol-gel chemistry in the presence of structure-directing amphiphilic triblock copolymers. Waveguiding in these structures is enabled by the use of low-refractive-index mesoporous SiO₂ supports, which were spin-cast and calcined on a silicon substrate.⁶² Due to the convenient preparation procedure, high photostability, and good adhesive properties for other materials, we expect that this type of support could find wide application where high-quality low-refractive-index materials are needed.

Laser dyes can be incorporated in a simple one-step synthesis. The surfactants that are present in the mesostructures in high concentrations (about 50% of the total weight) promote desirable dispersion of the rhodamine 6G dye species, thus reducing

unwanted dye aggregation, hence leading to low thresholds observed for these systems. The fact that nonionic surfactants with different compositions lead to materials with different optical properties suggests that the dye molecules are co-assembled with the surfactant and that they are not occluded—at least not exclusively—within the inorganic part.

Dye-doped block-copolymer/silica mesostructured composites are a promising class of compounds for optical applications. Their mesoscopically ordered structures, together with the inorganic/organic hybrid compositions, allow the local environment of included laser dye species to be controlled. Although this is one of the first reports on laser-like emission in mesostructured hosts, the relatively low thresholds observed are promising for the future. The optimization of these materials, such as through reduced dye self-absorption, the use of specifically designed surfactants and/or selection of different inorganic framework compositions, can be anticipated to lead to dye/host systems with improved optical properties and performance.

Acknowledgment. This work was supported by the National Science Foundation under grants DMR 96-34396 (G.D.S.) and CTS-9871970 (B.F.C.) and the U.S. Army Research Office under grant DAAH04-96-1-0443 (G.D.S.) and DAAH04-95-1-0102 (G.M.W.). We thank Dr. V. I. Srdanov and Dr. M. D. McGehee for help during the measurements and fruitful discussions. G.W. is on leave from the Karl-Franzens-University Graz and acknowledges support by the Fonds zur Förderung der wissenschaftlichen Forschung (J1634-CHE). Part of the work made use of the central facilities of the UCSB Materials Research Laboratory supported by the National Science Foundation (DMR-9632716). We thank BASF (Mt. Olive, NJ) for providing the block copolymer surfactants.

References and Notes

- Yanagisawa, T.; Shimizu, T.; Kuroda, K.; Kato, C. *Bull. Chem. Soc. Jpn.* **1990**, *63*, 988.
- Kresge, C. T.; Leonowicz, M. E.; Roth, W. J.; Vartuli, J. C.; Beck, J. S. *Nature* **1992**, *359*, 710.
- Beck, J. S.; Vartuli, J. C.; Roth, W. J.; Leonowicz, M. E.; Kresge, C. T.; Schmitt, K. D.; Chu, C. T.-W.; Olson, D. H.; Sheppard, E. W.; McCullen, S. B.; Higgins, J. B.; Schlenker, J. L. *J. Am. Chem. Soc.* **1992**, *114*, 10834.
- Bunker, B. C.; Rieke, P. C.; Tarasevich, B. J.; Campbell, A. A.; Fryxell, G. E.; Graff, G. L.; Song, L.; Liu, J.; Virden, J. W.; McVay, G. L. *Science* **1994**, *264*, 48.
- Sayari, A. *Chem. Mater.* **1996**, *8*, 1840.
- Corma, A. *Chem. Rev.* **1997**, *97*, 2373.
- Huo, Q.; Zhao, D.; Feng, J.; Weston, K.; Buratto, S. K.; Stucky, G. D.; Schacht, S.; Schüth, F. *Adv. Mater.* **1997**, *9*, 974.
- Marlow, F.; McGehee, M. D.; Zhao, D.; Chmelka, B. F.; Stucky, G. D. *Adv. Mater.* **1999**, *11*, 632.
- Avnir, D.; Levy, D.; Reisfeld, R. *J. Phys. Chem.* **1984**, *88*, 5956.
- Salin, F.; Le Saux, G.; Georges, P.; Brun, A.; Bagnall, C.; Zarzycki, J. *Opt. Lett.* **1989**, *14*, 785.
- McKiernan, J. M.; Yamanaka, S. A.; Dunn, B.; Zink, J. I. *J. Phys. Chem.* **1990**, *94*, 5652.
- Yanagi, H.; Hishiki, T.; Tobitani, T.; Otomo, A.; Mashiko, S. *Chem. Phys. Lett.* **1998**, *292*, 332.
- Deshpande, A.; Namdas, E. B. *Chem. Phys. Lett.* **1996**, *263*, 449.
- Kuwata-Gonokami, M.; Takeda, K.; Yasuda, H.; Ema, K. *Jpn. J. Appl. Phys.* **1992**, *31*, L99.
- Taniguchi, H.; Yamada, H.; Fujiwara, T.; Tanosaki, S.; Ito, H.; Morozumi, H.; Baba, M. *Jpn. J. Appl. Phys.* **1993**, *32*, L59.
- Kamada, K.; Sasaki, K.; Misawa, H.; Kitamura, N.; Masuhara, H. *Chem. Phys. Lett.* **1993**, *210*, 89.
- Zink, J. I.; Dunn, B.; Kaner, R. B.; Knobbe, E. T.; McKiernan, J. *ACS Symp. Ser.* **1991**, *455*, 541.
- Knobbe, E. T.; Dunn, B.; Fuqua, P. D.; Nishida, F. *Appl. Opt.* **1990**, *29*, 2729.
- Rottman, C.; Grader, G.; Hazan, Y. D.; Melchior, S.; Avnir, D. *J. Am. Chem. Soc.* **1999**, *121*, 8533.
- Behrens, P. *Angew. Chem., Int. Ed. Engl.* **1996**, *35*, 515.

- (21) Huo, Q.; Margolese, D. I.; Stucky, G. D. *Chem. Mater.* **1996**, *8*, 1147.
- (22) Huo, Q.; Margolese, D. I.; Ciesla, U.; Feng, P.; Gier, T. E.; Sieger, P.; Leon, R.; Petroff, P. M.; Schüth, F.; Stucky, G. D. *Nature* **1994**, *368*, 317.
- (23) Huo, Q.; Margolese, D. I.; Ciesla, U.; Demuth, D. G.; Feng, P.; Gier, T. E.; Sieger, P.; Firouzi, A.; Chmelka, B. F.; Schüth, F.; Stucky, G. D. *Chem. Mater.* **1994**, *6*, 1176.
- (24) Bagshaw, S. A.; Prouzet, E.; Pinnavaia, T. J. *Science* **1995**, *269*, 1242.
- (25) Zhao, D.; Feng, J.; Huo, Q.; Melosh, N.; Fredrickson, G. H.; Chmelka, B. F.; Stucky, G. D. *Science* **1998**, *279*, 548.
- (26) Yang, P.; Zhao, D.; Chmelka, B. F.; Stucky, G. D. *Chem. Mater.* **1998**, *10*, 2033.
- (27) Bruinsma, P. J.; Kim, A. Y.; Liu, J.; Baskaran, S. *Chem. Mater.* **1997**, *9*, 2507.
- (28) Lu, Y.; Ganguli, R.; Drewien, C. A.; Anderson, M. T.; Brinker, C. J.; Gong, W.; Guo, Y.; Soyez, H.; Dunn, B.; Huang, M. H.; Zink, J. I. *Nature* **1997**, *389*, 364.
- (29) Tolbert, S. H.; Schäffer, T. E.; Feng, J.; Hansma, P. K.; Stucky, G. D. *Chem. Mater.* **1997**, *9*, 1962.
- (30) Aksay, I. A.; Trau, M.; Manne, S.; Honma, I.; Yao, N.; Zhou, L.; Fenter, P.; Eisenberger, P. M.; Gruner, S. M. *Science* **1996**, *273*, 892.
- (31) Yang, H.; Kuperman, A.; Coombs, N.; Mamiche-Afara, S.; Ozin, G. A. *Nature* **1996**, *379*, 703.
- (32) Ryoo, R.; Ko, C. H.; Cho, S. J.; Kim, J. M. *J. Phys. Chem. B* **1997**, *101*, 10610.
- (33) Zhao, D.; Yang, P.; Melosh, N.; Feng, J.; Chmelka, B. F.; Stucky, G. D. *Adv. Mater.* **1998**, *10*, 1380.
- (34) Melosh, N. A.; Lipic, P.; Bates, F. S.; Wudl, F.; Stucky, G. D.; Fredrickson, G. H.; Chmelka, B. F. *Macromolecules* **1999**, *32*, 4332.
- (35) Göltner, C. G.; Henke, S.; Weissenberger, M. C.; Antonietti, M. *Angew. Chem., Int. Ed. Engl.* **1998**, *37*, 613.
- (36) Yang, P.; Deng, T.; Zhao, D.; Feng, P.; Pine, D.; Chmelka, B. F.; Whitesides, G. M.; Stucky, G. D. *Science* **1998**, *282*, 2244.
- (37) Yang, P.; Zhao, D.; Margolese, D. I.; Chmelka, B. F.; Stucky, G. D. *Nature* **1998**, *396*, 152.
- (38) Huang, M. H.; Dunn, B. S.; Soyez, H.; Zink, J. I. *Langmuir* **1998**, *14*, 7331.
- (39) Zhou, H. S.; Honma, I. *Adv. Mater.* **1999**, *11*, 683.
- (40) (a) Wirnsberger, G.; Stucky, G. D. *Eur. J. Phys. Chem.* **2000**, *1*, 90. (b) Wirnsberger, G.; Stucky, G. D. *Chem. Mater.* **2000**, *12*, 2525.
- (41) Honma, I.; Zhou, H. S. *Chem. Mater.* **1998**, *10*, 103.
- (42) Wu, J.; Gross, A. F.; Tolbert, S. H. *J. Phys. Chem. B* **1999**, *103*, 2374.
- (43) Dag, Ö.; Ozin, G. A.; Yang, H.; Reber, C.; Bussiere, G. *Adv. Mater.* **1999**, *11*, 474.
- (44) Yang, P.; Wirnsberger, G.; Huang, H. C.; Cordero, S. R.; Scott, B.; McGehee, M. D.; Deng, T.; Whitesides, G. M.; Chmelka, B. F.; Buratto, S. K.; Stucky, G. D. *Science* **2000**, *287*, 465.
- (45) Xia, Y.; Whitesides, G. M. *Angew. Chem., Int. Ed. Engl.* **1998**, *37*, 551.
- (46) Xia, Y.; Whitesides, G. M. *Annu. Rev. Mater. Sci.* **1998**, *28*, 153.
- (47) Xia, Y.; Rogers, J. A.; Paul, K. E.; Whitesides, G. M. *Chem. Rev.* **1999**, *99*, 1823.
- (48) Trau, M.; Yao, N.; Kim, E.; Xia, Y.; Whitesides, G. M.; Aksay, I. A. *Nature* **1997**, *390*, 674.
- (49) We take the threshold as the value where the initial fwhm observed at low pumping energies has decreased to half of that value.
- (50) Siegman, A. E. *Lasers*; University Science Books: Mill Valley, CA, 1986.
- (51) Silfvast, W. T. *Laser Fundamentals*; Cambridge University Press: Cambridge, 1996.
- (52) Vlasov, Yu. A.; Luterova, K.; Pelant, I.; Hönerlage, B.; Astratov, V. N. *Appl. Phys. Lett.* **1997**, *71*, 1616.
- (53) McGehee, M. D.; Gupta, R.; Veenstra, S.; Miller, K. E.; Díaz-García, M. A.; Heeger, A. J. *Phys. Rev. B* **1998**, *58*, 7035.
- (54) Gupta, R.; Stevenson, M.; Dogariu, A.; McGehee, M. D.; Park, J. Y.; Srdanov, V.; Heeger, A. J.; Wang, H. *Appl. Phys. Lett.* **1998**, *73*, 3492.
- (55) Berggren, A.; Dodabalapur, A.; Slusher, R. E. *Appl. Phys. Lett.* **1997**, *71*, 2230.
- (56) Rahn, M. D.; King, T. A. *Appl. Opt.* **1995**, *34*, 8260.
- (57) Dunn, B.; Zink, J. I. *J. Mater. Chem.* **1991**, *1*, 903.
- (58) Wirnsberger, G.; Stucky, G. D. In preparation.
- (59) Zhou, H. S.; Sasabe, H.; Honma, I. *J. Mater. Chem.* **1998**, *8*, 515.
- (60) Ganschow, M.; Wöhrle, D.; Schulz-Ekloff, G. *J. Porphyrins Phthalocyanines* **1999**, *3*, 299.
- (61) *Topics in Applied Physics, Dye Lasers*, Vol. 1; Schäfer, F. P., Ed.; Springer-Verlag: Berlin, 1977, and references therein.
- (62) We also patterned mesostructured waveguides directly on silicon. The threshold increased to 100 kW cm⁻² (dye concentration of 0.58 wt %).